Diffuse Whistler Mode Waves Detected by Kaguya in Lunar Polar Region

Tomoko Nakagawa[1,1], Futoshi Takahashi[2,2], Hisayoshi Shimizu[3,3], and Yoshifumi Saito[4,4]

[1]Tohoku Institute of Technology
[2]Kyushu University
[3]University of Tokyo
[4]Institute of Space & Astronautical Science

November 30, 2022

Abstract

The solar wind particles reflected by the lunar magnetic field are the major energy source of electromagnetic wave activities, such as the 100 s magnetohydrodynamic waves and the 1 Hz whistler-mode waves generated by protons and the non-monochromatic whistler-mode waves generated by mirror-reflected electrons. Kaguya found a new type of whistler-mode waves at 100 km altitude above the polar regions of the moon with a broad frequency range of 1–16 Hz. The waves appear diffuse in both the time and frequency domains, and their occurrence is less sensitive to the magnetic connection to the lunar surface. The polarization is right-handed with respect to the background magnetic field, and the wave number vector is nearly parallel to the magnetic field perpendicular to the solar wind flow. The diffuse waves are thought to be generated by the solar wind ions reflected by the lunar magnetic field through cyclotron resonance. The resonant ions are expected to have a velocity component parallel to the magnetic field larger than the solar wind bulk speed; however, such ions were not always simultaneously detected by Kaguya. The waves may have been generated above the dayside of the moon and then propagated along the magnetic field being convected by the solar wind to reach the polar regions to be detected by Kaguya.

Diffuse Whistler-Mode Waves Detected by Kaguya in the Lunar Polar Region

T. Nakagawa[1], F. Takahashi[2], H. Shimizu[3], and Y. Saito[4]

[1]Department of Information and Communication Engineering, Tohoku Institute of Technology, Miyagi, 982-8577 Japan.

[2]Department of Earth and Planetary Sciences, Faculty of Science, Kyushu University, Fukuoka 819-0395.

[3]Earthquake Research Institute, University of Tokyo, Tokyo 113-0032, Japan.

[4]Institute of Space and Astronautical Science, Japan Aerospace Exploration Agency, Kanagawa, 229-8510 Japan.

Corresponding author: Tomoko Nakagawa (nakagawa@tohtech.ac.jp)

Key Points:

- Diffuse emission of whistler-mode waves from 1 Hz to 16 Hz is found over the polar regions of the moon in the solar wind.
- Right-hand polarized waves propagate parallel to the background magnetic field without a significant Doppler shift.
- The waves are thought to be generated by the ions reflected by the moon and propagate along field lines convected by the solar wind.

Abstract

The solar wind particles reflected by the lunar magnetic field are the major energy source of electromagnetic wave activities, such as the 100 s magnetohydrodynamic waves and the 1 Hz whistler-mode waves generated by protons and the non-monochromatic whistler-mode waves generated by mirror-reflected electrons. Kaguya found a new type of whistler-mode waves at 100 km altitude above the polar regions of the moon with a broad frequency range of 1–16 Hz. The waves appear diffuse in both the time and frequency domains, and their occurrence is less sensitive to the magnetic connection to the lunar surface. The polarization is right-handed with respect to the background magnetic field, and the wave number vector is nearly parallel to the magnetic field perpendicular to the solar wind flow. The diffuse waves are thought to be generated by the solar wind ions reflected by the lunar magnetic field through cyclotron resonance. The resonant ions are expected to have a velocity component parallel to the magnetic field larger than the solar wind bulk speed; however, such ions were not always simultaneously detected by Kaguya. The waves may have been generated above the dayside of the moon and then propagated along the magnetic field being convected by the solar wind to reach the polar regions to be detected by Kaguya.

Plain Language Summary

Unlike Earth, the moon is not shielded by a global magnetic field; hence, solar wind particles can access the lunar surface. Although most of these particles are absorbed by the surface, a small fraction is scattered by the surface or reflected by intense lunar magnetic fields (magnetic anomalies) back into the solar wind and can become an energy source of wave activities. The protons reflected by these magnetic anomalies generate 0.01 Hz ultra-low frequency waves and 1 Hz electron cyclotron waves. The electrons reflected by the lunar magnetic field form a field-aligned beam that generates broadband electromagnetic waves, whose detection depends on the magnetic connection of spacecraft to the lunar surface. Kaguya found a new type of electromagnetic waves with a broad frequency range like the waves generated by the electrons, but less sensitive to the magnetic connection like the waves generated by the reflected protons. These electromagnetic waves are preferentially observed above the polar region of the moon, not above intense magnetic anomalies. They are thought to be generated by the solar wind ions reflected by the lunar magnetic fields and propagate along the solar wind magnetic field to the polar region being convected down the solar wind flow.

1 Introduction

Solar wind particles directly hit the moon due to the lack of a global-scale magnetic field or a dense atmosphere. Most of them are absorbed by the lunar surface, leaving a plasma void, called a lunar wake, on the downstream side (Lyon et al., 1967; Colburn et al., 1967; Schubert & Lichtenstein, 1974; Bosqued et al., 1996; Ogilvie et al., 1996). A small fraction of these particles is scattered, reflected, or diffracted by the lunar surface or its crustal magnetic field. Observations from Kaguya and Chandrayaan-1 revealed that 0.1–1% of the incident plasmas is backscattered by the lunar surface, while 10–50% is reflected by the local crustal fields, called magnetic anomalies (Saito et al., 2008, 2010; Lue et al., 2011). Above intense magnetic anomalies, the deceleration of ions and the acceleration of electrons parallel to the magnetic field were observed together with heating of reflected ions (Saito et al., 2012). Chandrayaan-1 and IBEX showed that up to 20% of the incident solar wind particles is backscattered in the form of energetic neutral hydrogen atoms with energy of several tens of eV. Some of the particles experience charge exchange with ambient plasmas and begin to behave as reflected protons thereafter (McComas et al., 2009; Wieser et al., 2009, 2011; Poppe et al., 2014; Bhardwaj et al., 2015).

Backscattered, reflected, or diffracted particles are the main source of various wave activities (Harada et al., 2015; Nakagawa, 2016; Harada & Halekas, 2016, and references therein). The most prominent waves in the low-frequency range are the 0.01 Hz ultra-low-frequency waves (Nakagawa et al., 2012) and the 1 Hz whistler-mode waves (Halekas et al., 2006b; Tsugawa et al., 2011) generated by the reflected protons through cyclotron resonance with solar wind magnetohydrodynamic waves or the whistler-mode waves propagating against the solar wind flow. Figures 1a and 1b show typical examples of such waves. They are Doppler-shifted and detected as narrowband, often left-handed polarized waves with respect to the background magnetic field. Their occurrence is not sensitive to the magnetic connection between spacecraft and the lunar surface estimated from the intersection of the linearly extrapolated line of force of the magnetic field observed at Kaguya and the lunar surface. The red and blue bars at the bottom of each spectrum in Figure 1 indicate the magnetic connection to the dayside and nightside surfaces of the moon, respectively. The narrowband waves in Figures 1a and 1b were continuously observed, while the magnetic connection was intermittent. The detection was not controlled by the magnetic connection, suggesting that they were generated by protons with a large gyro radius.

Another kind of prominent wave found around the moon is the non-monochromatic whistler-mode waves in the extremely low frequency (ELF) range of 0.1 Hz to 10 Hz (Nakagawa et al., 2011; Tsugawa et al., 2012). They are often observed on the dayside of the moon, and their occurrence is severely controlled by the magnetic connection of spacecraft to the lunar surface. Figure 1c shows an example of a non-monochromatic whistler-mode wave. The broadband emission was mainly observed when Kaguya was magnetically connected to the dayside surface of the moon. The wave activity was reduced at around 3:08, 3:30, and 3:37–3:42 when the magnetic connection was lost and immediately recovered as the connection recovered. The wave intensity enhanced when the spacecraft was magnetically connected to the magnetic anomalies, suggesting that the energy source was the electrons bound to the magnetic field lines within a

small gyroradius. The waves are thought to be generated by the mirror-reflected electrons above the lunar crustal magnetic field (Saito et al., 2012).

These low-frequency waves around the moon can be categorized into two types: (1) monochromatic waves with a sharp boundary in the frequency domain not sensitive to the magnetic connection to the lunar surface; and (2) non-monochromatic waves with a sharp boundary in the time domain sensitive to the magnetic connection to the lunar surface. In addition to these known waves, a new type of diffuse ELF wave was also found by Kaguya above the polar region of the moon. It is a diffuse emission both in the frequency and time domains. The waves appeared in a broad frequency range from 1 Hz to 16 Hz like the ELF waves generated by the reflected electrons. However, different from that of the electron-generated ELF waves, their occurrence was not sensitive to the magnetic connection to the lunar surface like the waves generated by protons. Their generation mechanism is not known. This paper reports the characteristics and the possible generation mechanism of the newly found diffuse ELF waves.

2 Data

The magnetic field and the plasma data used in this study were obtained by Lunar MAGnetometer (LMAG) and Plasma energy Angle and Composition Experiment (PACE) of the MAgnetic field and Plasma experiment (MAP) (Saito et al., 2008, 2010; Tsunakawa et al., 2010; Shimizu et al., 2008) onboard Kaguya on its polar orbit around the moon during the period from January 1, 2008 to September 30, 2008. The spacecraft altitude was approximately 100 km above the lunar surface (Kato et al., 2010). The period of orbital motion was approximately 2 h.

The magnetic field vectors obtained by the LMAG at 32 Hz sampling frequency (Takahashi et al., 2009) were Fourier transformed every 32 s. Minimum variance analysis (Sonnerup and Cahill, 1967) was applied to each Fourier component to obtain the direction of the wavenumber vector **k**. The **k** vector was assumed to be parallel to the minimum direction. The intermediate and maximum variance components were separated into left- or right-handed polarized components with respect to the background magnetic field. The sense of rotation (polarization) with respect to the background magnetic field of the wave is defined as $(B_L^2 - B_R^2)/(B_L^2 + B_R^2)$, where B_L and B_R are the amplitudes of the left- or right-handed components, respectively.

The three-dimensional (3D) energy distributions of the ions and the electrons were obtained using four sensors of the MAP–PACE, Ion Energy Analyzer (IEA), and Ion Mass Analyzer (IMA) for the ions and Electron Spectrum Analyzer (ESA)-S1 and ESA-S2 for the electrons. The IMA and ESA-1 sensors were installed on the nadir-looking panel of the spacecraft to detect the particles coming from the moon, while the IEA and ESA-2 sensors were installed on the zenith-looking panel. The energy range was 7 eV/q–29 keV/q for the IEA, 7 eV/q–28 keV/q for the IMA, 6 eV–9 keV for the ESA-S1, and 9 eV–16 keV for the ESA-S2 (Saito et al., 2010). The densities of the ions observed by the IMA and the IEA were separately calculated from each distribution function (Saito et al., 2010) and combined to obtain the total ion density.

The upstream solar wind condition was monitored using Level 2 data from the Solar Wind Electron, Proton, and Alpha Monitor (SWEPAM) onboard the Advanced Composition

Explorer (ACE) spacecraft. The data were extracted from the OMNI data set of NASA/GSFC through OMNIWeb Plus.

3 Observations

3.1 Diffuse ELF waves in the solar wind

Figure 2 shows an example of the diffuse ELF waves found by Kaguya on March 8, 2008 when the moon was in the solar wind (Figure 3a). A diffuse emission was observed in the frequency range of 4 Hz to 16 Hz during the period from 7:03 to 7:13 when the spacecraft was above the southern polar region of the moon (Figures 2f and 3c–d). In the previous spacecraft evolution, faint, but similar waves were seen from 5:11 to 5:17 in a range of 6–12 Hz in the same region over the south pole. The frequency range was between the ion and electron cyclotron frequencies of 0.075 Hz and 0.14 kHz (for the magnetic field of 4.9 nT at 7:05). The ion bulk density calculated from the velocity distribution functions from the IEA and the IMA was approximately 8.0×10^{6} m^{-3} during the period, which resulted in a lower hybrid frequency of 3.2 Hz. The diffuse ELF wave frequency was close to the lower hybrid frequency. Figure 4 shows a comparison of the cross-cut spectrum of the power density of the diffuse wave (Figure 4b) with that for a quiet period (Figure 4a). The power density enhanced over a wide range from 4 Hz to 16 Hz.

The diffuse waves were detected when Kaguya was not magnetically connected to the lunar surface, as indicated by the blanks in Figure 2b. The background magnetic field $\mathbf{B}_0$ was almost in the y_{sse} direction of the selenocentric solar ecliptic (sse) coordinate system during the diffuse ELF wave detection (Figure 2g).

Figure 2c shows the sense of polarization in the spacecraft frame of reference for each Fourier component, whose power density was greater than 5×10^{-3} $\mathrm{nT}^2/\mathrm{Hz}$. The red color in the figure indicates the right-handed polarization with respect to the background magnetic field. The diffuse ELF wave polarization was predominantly right-handed with respect to the background magnetic field. The wave number vector **k** of the diffuse ELF wave was nearly parallel to the background magnetic field $\mathbf{B}_0$. Figure 2d shows the angle $\theta_{\mathbf{k}\cdot\mathbf{B}_0}$ between vectors **k** and $\mathbf{B}_0$. The red color indicates that vector **k** was parallel to $\mathbf{B}_0$. The polarization and propagation directions suggested that the diffuse ELF emissions were whistler-mode waves. No significant Doppler shift was expected because the **k** vector was nearly perpendicular to the bulk flow of the solar wind in the x_{sse} direction (Figure 2e).

The diffuse waves were not detected above intense magnetic anomalies. Figure 5 shows the Kaguya position during the detection of the diffuse wave projected onto a color-coded map of the crustal magnetic field magnitude at the lunar surface calculated from the Kaguya observation (Tsunakawa et al., 2015). No intense magnetic field was found at the Kaguya position. Most of the intense magnetic anomalies extended sunward and equatorward of Kaguya.

As shown in Figure 2g, the diffuse ELF waves were observed on the positive gradient of the magnitude toward a lunar external magnetic enhancement (LEME, see Halekas et al., 2006a) with a peak magnitude at 7:13. The diffuse waves disappeared at the LEME peak. Another type of low-frequency wave was observed at around 0–4 Hz at the LEME. However, its properties of mixed polarization and direction of wave number vectors nearly perpendicular to the magnetic field were quite different from the diffuse ELF waves.

Figures 2h and 2i show the energy–time spectra of the ions detected by the IEA and the IMA sensors of the MAP–PACE, respectively. During the diffuse ELF wave detection, the IMA observed a bunch of protons reflected by a crustal field from 7:02 to 7:10 in the energy range of 0.1 keV to 1 keV, but the start and end times of the reflected ions were not exactly the same as those of the diffuse ELF waves. The IEA consistently detected incident solar wind ions centered at 0.5 keV with the ACE observation of 330 km/s at 1.52×10^{6} km upstream in the solar wind shifted by approximately 1 h for traveling the distance. The upstream number density of the solar wind at the ACE was 2×10^{7} m^{-3}, which was higher than the nominal value of the solar wind. The IMA detected another bunch of reflected protons from 6:53 to 7:00, which were not accompanied by diffuse ELF waves.

3.2 Diffuse ELF waves in the magnetosheath

Figure 6 shows another diffuse ELF event found in Earth's magnetosheath. Kaguya was on the nightside of the terminator, but was exposed to the magnetosheath flow (Figures 7c, 7d and 8). A diffuse emission was found in a frequency range from 1 Hz to 8 Hz during the period from 20:40 to 21:00 on June 14, 2008 above the northern polar region of the moon. The emission appeared diffuse both in the time and frequency domains, making a clear contrast with the broadband emissions with a sharp appearance and a mixed polarization observed from 21:00 to 22:00.

The observed frequency of 1–8 Hz corresponded to 3–24 times of the ion cyclotron frequency of 0.34 Hz calculated from the magnitude of the background magnetic field of 19.4–22.1 nT. Figure 6 presents three lanes of falling tone starting at around 20:40, 20:45, and 20:50. The polarization was right-handed with respect to the background magnetic field, and the **k** vector was again nearly parallel to the magnetic field. The **k** vector was nearly perpendicular to the bulk flow of the magnetosheath plasma (Figure 6e) because the magnetic field was almost in southward direction (Figure 6g). Thus, Doppler-shift effect was supposed to be small.

Throughout the diffuse ELF wave event, Kaguya was magnetically connected to the lunar surface (Figure 6b). Figure 8 shows how the line of force of the magnetic field at Kaguya was connected to the moon. The line of force of the magnetic field was connected to the lunar surface just below the spacecraft, where no intense crustal magnetic field was found. A cluster of intense crustal fields is instead seen at the lower latitude, upstream side (orange line pointing to the sun at the lower left) of the spacecraft. Figure 9 depicts the polar view in the Lambert azimuthal equal area projection.

The diffuse appearance and insensitiveness to the magnetic connection suggest that the emission was generated by ions. An attempt was made to search for the ions that would generate the waves in the energy–time spectrogram of the ions detected by the IMA (Figure 6i), but it was difficult to distinguish the reflected ions from the incident solar wind component because the latter also entered the IMA sensor of Kaguya on this orbit just behind the terminator. The ion energy typically ranged from 0.5 keV to 2.0 keV, consistent with the bulk speed of 400 km/s of the sheath flow calculated from the distribution functions obtained by the IMA and the IEA during the period of the diffuse ELF event. The number density of the ions calculated from the IEA and IMA observations was 1×10^{7} m^{-3}.

4 Discussion

4.1 Summary of observation

The properties of the diffuse ELF waves observed by Kaguya around the moon are summarized as follows:
1) The waves were magnetic fluctuations in a frequency range of 1 Hz to 16 Hz between the local ion and electron cyclotron frequencies.
2) The waves were right-hand polarized with respect to the background magnetic field.
3) The wave number vector was nearly parallel to the background magnetic field.
4) The waves were detected irrespective of the magnetic connection to the lunar surface.
5) The waves were preferentially observed in the polar region.

4.2 Possible explanation for the broad frequency range

Considering the frequency range and the right-handed polarization with respect to the background magnetic field, the diffuse ELF waves are thought to be whistler-mode waves propagating nearly parallel to the background magnetic field. The energy source is supposed to be the ions reflected by the crustal magnetic field, which have broader energy and angular distributions compared to the incident solar wind (Saito et al., 2010, 2012). They would form a ring-beam distribution in the velocity space that can generate whistler-mode waves through cyclotron resonance (Gary, 1991).

The broadband, diffuse emission is expected to be caused by the ineffectiveness of the Doppler shift. If the wave number vector $\mathbf{k}$ is antiparallel to the solar wind velocity $\mathbf{V}_{sw}$, the resonant waves will be heavily Doppler-shifted, and the observed bandwidth would be narrowed with reversed polarization (Figure 10a). The dashed lines in Figure 10 represent the Doppler-shift relationship between the angular frequencies ω in the solar wind frame and ω_{OBS} in the spacecraft frame of reference

$$\omega + \mathbf{k} \cdot \mathbf{V}_{SW} = \omega_{OBS}. \quad (1)$$

The polarization ω, which is positive (negative) for the right-handed (left-handed) polarization, would be reversed if the $\mathbf{k} \cdot \mathbf{V}_{SW}$ term is large. In contrast, if the wave number vector $\mathbf{k}$ is nearly perpendicular to the solar wind flow, the term $\mathbf{k} \cdot \mathbf{V}_{SW}$ would be small and would not narrow the bandwidth or reverse the polarization (Figure 10b).

The real resonance occurred at a higher frequency than that illustrated in Figure 10. The resonant conditions will be investigated in the next section by using the dispersion curves drawn with the parameters observed.

4.3 Dispersion relation and resonant condition

Figure 11 shows the dispersion relation $\omega(k)$ of parallel propagating whistler-mode waves drawn with the parameters of the diffuse ELF event observed on July 14, 2008. The magnitude of the magnetic field was 22.1 nT at 20:58. The plasma density was assumed to be equal to the ion density 1×10^{7} m^{-3} calculated from the 3D velocity distribution functions obtained from the IEA and IMA sensors of the PACE. The observed 1–8 Hz frequency normalized by the ion cyclotron frequency of 0.34 Hz corresponded to 3–24 Ω_i. The wave number vector was assumed to be parallel to the background magnetic field.

The dashed lines in Figure 11 represent the Doppler-shift equation (Eq. (1)) for the upper and lower boundaries of the observed frequency. The -100 km/s of inclination was calculated from the bulk speed of 400 km/s observed by the MAP–PACE on the assumption that the wave was propagating away from the moon, and the $\mathbf{k}$ vector was antiparallel to the background magnetic field $(5.6,\ -7.6,\ -20.0)$ nT. The dispersion curve intersected the upper and lower boundaries at $(\omega, k) = (21\ \Omega_i,\ 9\times10^3\Omega_i c^{-1})$ and $(2\ \Omega_i,\ 3\times10^3\Omega_i c^{-1})$, respectively. Thus, the whistler-mode wave frequency in the sheath flow frame was estimated to range from 0.6 Hz to 7 Hz, and the wavelength was between 100 km and 300 km.

In Figure 11, the cyclotron resonance condition of the reflected ions with velocity $\mathbf{V}_R$

$$\omega + \mathbf{k}\cdot\mathbf{V}_{SW} - \mathbf{k}\cdot\mathbf{V}_R = -\Omega_i \tag{2}$$

is represented by the gray solid lines with positive inclinations. Three lines represent the ions with a parallel speed $V_{\parallel} \equiv (\mathbf{k}\cdot\mathbf{V}_{SW} - \mathbf{k}\cdot\mathbf{V}_R)/|\mathbf{k}|$ of 440 km/s (1 keV), 620 km/s (2 keV), and 760 km/s (3 keV) as a measure of the energy of the solar wind (or magnetosheath) protons. A line with a very small inclination does not intersect the curve in a positive ω range. That is, very slow ions cannot be resonant with the whistler-mode waves. The line for the 1 keV ions intersects the dispersion curve at two points around $1\,\Omega_i$ and $4\,\Omega_i$, and the latter agrees with the observed frequency range. This is different from the illustrations in Figure 10, in which the resonance is assumed to be at a lower frequency. The lower limit of the possible intersection would be at around $2\,\Omega_i$, consistent with the lowest frequency of the detected diffuse ELF waves in the sheath flow frame.

To account for the upper boundary of the observed frequency, we need $V_{\parallel}$ as large as 760 km/s (3 keV), which is approximately $\sqrt{3}$ times faster than the solar wind bulk speed. In Figure 6i, the upper boundary of the ion energy was approximately 2 keV in the spacecraft frame of reference. The reflected ions with velocity $\mathbf{V}_R$ in the spacecraft frame had velocity $\mathbf{V}_R - \mathbf{V}_{sw}$ in the solar wind (or magnetosheath flow) frame of reference. However, in this event, the wave number vector $\mathbf{k}$ is nearly perpendicular to the solar wind flow, and the term $\mathbf{k}\cdot\mathbf{V}_{sw}$ does not contribute to $V_{\parallel}$. The reflected ions must have a higher velocity than the solar wind speed to have the parallel component $V_{\parallel}$ as estimated.

Figure 6 shows a falling tone structure of the diffuse ELF waves. The magnetic field, plasma density, and bulk velocity were stable during the period. Any distinct feature, which might correspond to the falling tone structure, was searched for in the MAP–PACE data, but no such feature was found. The frequency decrease can be interpreted as a decrease in the parallel velocity component of the reflected ions responsible for the wave generation. Whether it was temporal or spatial variation remains unclear. During the 5 min interval of the three lanes of falling tone, Kaguya traveled approximately 15° in longitude. The direction of the velocities of the reflected ions may have varied depending on the distance from their reflection point, but it is not understood why the falling tone repeatedly appeared.

Figure 12 depicts the Doppler-shift relation of the observed frequencies overlaid on a dispersion relation $\omega(k)$ of the parallel propagating whistler wave for the March 8, 2008 diffuse ELF event. The plasma density was assumed to be equal to the ion density $8\times10^6\,\mathrm{m}^{-3}$ calculated from the velocity distribution measurements by the IEA and the IMA. The magnetic field magnitude of 4.9 nT at 07:05 was employed. The observed frequency 4–16 Hz normalized by the

ion cyclotron frequency of 0.075 Hz corresponded to 54–210 Ω_i. Note that the upper boundary of the frequency range was limited by half of the sampling rate (32 Hz) of the magnetic field observation.

The Doppler shift was small for this case. The bulk velocity of the solar wind calculated from the MAP–PACE observation was 250 km/s, and the velocity component parallel to the background magnetic field (0.47, 4.6, 1.5) nT was as small as 24 km/s. The lines of the Doppler-shift equation (Eq. (1)) with positive and negative inclinations were drawn for two possible propagation directions parallel or antiparallel to the magnetic field. The frequency in the solar wind frame fell in the range from $54 \pm 8\Omega_i$ (4 ± 0.3 Hz) to $210 \pm 10\Omega_i$ (16 ± 0.75 Hz). The wave number $|\mathbf{k}|$ was estimated to be $6\times10^4 |\Omega_i|/c$ –$1.2\times10^5 |\Omega_i|/c$, corresponding to the wavelength from 66 km to 33 km.

The gray lines in Figure 12 depict the cyclotron resonance conditions for the ions with three different values of $V_\parallel$ = 310 km/s (0.5 keV), 440 km/s (1 keV), and 540 km/s (1.5 keV). To account for the observed frequency range, the ions should have velocity components $V_\parallel$ in the range of 310 km/s–540 km/s, which is approximately $1–\sqrt{3}$ times larger than that of the incident solar wind.

4.4 Possible generation mechanism

The velocity component $V_\parallel$ of the reflected ions must be larger than the solar wind bulk speed to be resonant with the observed waves. On the contrary, in a magnetic field perpendicular to the solar wind flow, the velocity component $V_\parallel$ cannot exceed the incident speed. The speed of the reflected ions can be two times as large as the incident speed in the solar wind frame of reference, but it contributes a perpendicular component $V_\perp$, not a parallel component $V_\parallel$. The parallel component $V_\parallel$ is maximized when the ions are reflected into the direction parallel to the magnetic field with the same speed as the initial speed. We need an initial speed larger than the solar wind bulk speed to obtain fast enough $V_\parallel$. High-energy components and the core component of the solar wind ions must be reflected into the magnetic field direction.

Another possibility is that the diffuse waves were generated in the upstream flow, not at the Kaguya position. Figure 2i shows a slight disagreement in the appearance/disappearance time between the diffuse waves and the reflected ions. Bunches of reflected protons at around 6:55 and 4:55 were not accompanied by the diffuse ELF waves. In Figures 8 and 9, we can hardly find magnetic anomalies that would reflect incident ions. The ions responsible for the diffuse wave generation might not be detected at the Kaguya position.

Figure 13 schematically illustrates the wave generation and propagation. The solar wind ions reflected by the lunar magnetic field can have a large velocity component $V_\perp$ perpendicular to the magnetic field (Saito et al., 2010) and a large gyroradius (Nishino et al., 2009, 2013). A whistler-mode wave was generated in the upstream solar wind by the reflected ions and began propagating along the magnetic field line convected by the solar wind flow. The slower wave components might crash into the lunar surface before they reach the limb. Only the wave component that is fast enough can propagate to the limb (polar region or the terminator) to be detected by Kaguya. The group velocity of the whistler-mode wave is higher than the phase

velocity that determines the resonant condition; hence, the resonant ions may not reach Kaguya above the polar region. The ions might hit the moon to be absorbed by the surface or reflected by the lunar magnetic field again into directions that are different from those of the wave. Multiple reflections might increase the ion velocity by the self-pickup process (Saito et al., 2010).

5 Conclusions

Diffuse, right-hand polarized whistler-mode waves propagating parallel to the magnetic field were found by Kaguya over the polar regions of the moon. These waves are thought to be generated by the solar wind ions reflected by the lunar magnetic field into directions perpendicular to the solar wind flow. Due to ineffectiveness of the Doppler shift, the polarization was not reversed, and the frequency range was not narrowed. The reflected ions resonant with the whistler-mode waves must have a higher velocity component parallel to the magnetic field than the solar wind bulk speed, although such higher-energy ions were not always simultaneously detected. A possible explanation for this is that the cyclotron resonance occurs upstream in the solar wind above the lunar magnetic anomaly, and the waves propagate along the magnetic field to the polar region during the travel time of the solar wind to pass from the resonant site to the observer at the polar region.

Acknowledgments

The authors thank the Kaguya MAP-LMAG and MAP-PACE teams for the Kaguya magnetic field and plasma particle data. The Kaguya MAP-LMAG and MAP-PACE data are available at Kaguya (SELENE) Data Archive (http://l2db.selene.darts.isas.jaxa.jp/index.html.en). The authors also thank the ACE SWEPAM instrument team and the ACE Science Center for providing the ACE data. Interplanetary magnetic field parameter (MAG) and solar wind parameter (SWEPAM) data obtained by ACE are available at the ACE Science Center (http://www.srl.caltech.edu/ACE/ASC/index.html). T. Nakagawa thanks Yoshiki Sugata and Sho Ito for their contribution in event finding and examination of spatial distribution and solar wind condition. The authors declare that they have no conflicts of interests. This work was supported by JSPS KAKENHI Grant Number 18K03727.

References

Bhardwaj, A., Dhanya, M. B., Alok1, A., Barabash, S., Wieser, M., Futaana, Y., Wurz, P., Vorburger, A., Holmström, M., Lue, C., Harada, Y., & Asamura, K. (2015), A new view on the solar wind interaction with the Moon, Geosci. Lett. 2:10, DOI 10.1186/s40562-015-0027-y.

Bosqued, J. M., Lormant, N., R`eme, H., d'Uston, C., Lin, R. P., Anderson, K. A., Carlson, C. W., Ergun, R. E., Larson, D., McFadden, J., McCarthy, M. P., Parks, G. K., Sanderson, T. R., & Wenzel, K.-P. (1996), Moon solar wind interaction: First results from the WIND/3DP experiment, Geophys. Res. Lett., 23, 1259–1262, doi:10.1029/96GL00303.

Colburn, D.S., R. G. Currie, J. D. Mihalov, C. P. Sonett (1967), Diamagnetic solar-wind cavity discovered behind moon, Science, 158, 1040–1042.

Gary, S. P. (1991), Electromagnetic ion/ion instabilities and their consequences in space plasmas - A review, Space Science Reviews, 56, p. 373 – 415, doi:10.1007/BF00196632.

Halekas, J. S., Brain, D. A., Mitchell, D. L., Lin, R. P., Harrison, L. (2006a), On the occurrence of magnetic enhancements caused by solar wind interaction with lunar crustal fields. Geophys. Res. Lett. 33, L01201, doi:10.1029/2006GL025931.

Halekas, J. S., Brain, D. A., Mitchell, D. L., & Lin, R. P. (2006b), Whistler waves observed near lunar crustal magnetic sources. Geophysical Research Letters, 33, L22104. doi:10.1029/2006GL027684.

Harada, Y., Halekas, J. S., Poppe, A. R., Tsugawa, Y., Kurita, S., & McFadden, J. P. (2015), Statistical characterization of the foremoon particle and wave morphology: ARTEMIS observations. J. Geophys. Res. Space Physics, 120, 4907– 4921. doi: 10.1002/2015JA021211.

Harada, Y., & Halekas, J. S. (2016), Upstream Waves and Particles at the Moon, in *Low-Frequency Waves in Space*, chap. 18, pp. 307–322, John Wiley Sons, Inc, Hoboken, NJ, doi: 10.1002/9781119055006.

Kato, M., Sasaki, S., Takizawa, Y. & the Kaguya project team (2010), The Kaguya mission overview, *Space Sci. Rev.*, 154, 3–19, doi:10.1007/s11214-010-9678-3.

LRO Project and Lunar Geodesy and Cartography Working Group (2008), A standardized lunar coordinate system for the Lunar Reconnaissance Orbiter and lunar datasets, LRO Project and LGCWG White Paper, version 5, Goddard Space Flight Center, National Aeronautics and Space Administration, http://lunar.gsfc.nasa.gov/library/LunCoordWhitePaper-10-08.pdf.

Lyon, E. F., Bridge, H. S., & Binsack, J. H. (1967), Explorer 35 plasma measurements in the vicinity of the Moon, J. Geophys. Res., 72(23), 6113– 6117, doi:10.1029/JZ072i023p06113.

Lue, C., Futaana, Y., Barabash, S., Wieser, M., Holmström, M., Bhardwaj, A., Dhanya, M. B., & Wurz, P. (2011), Strong influence of lunar crustal fields on the solar wind flow, Geophys. Res. Lett., 38, L03202, doi:10.1029/2010GL046215.

McComas, D. J., Allegrini, F., Bochsler, P., Frisch, P., Funsten, H. O., Gruntman, M., Janzen, P. H., Kucharek, H., Möbius, E., Reisenfeld, D. B., & Schwadron, N. A. (2009), Lunar backscatter and neutralization of the solar wind: First observations of neutral atoms from the Moon, Geophys. Res. Lett., 36, DOI: 10.1029/2009GL038794.

Nakagawa, T. (2016), ULF/ELF waves in the near-Moon space, in *Low-Frequency Waves in Space*, chap. 17, pp. 295–306, John Wiley Sons, Inc, Hoboken, NJ, doi:10.1002/9781119055006.

Nakagawa, T., Takahashi, F., Tsunakawa, H., Shibuya, H., Shimizu, H., & Matsushima, M. (2011). Non-monochromatic whistler waves detected by Kaguya on the dayside surface of the moon. Earth, Planets and Space, 63, 37–46, doi:10.5047/eps.2010.01.005

Nakagawa, T., Nakayama, A., Takahashi, F., Tsunakawa, H., Shibuya, H., Shimizu, H., & Matsushima, M. (2012). Large-amplitude monochromatic ULF waves detected by Kaguya at the moon. Journal of Geophysical Research, 117, A04101, doi:10.1029/2011JA017249.

Nishino, M. N., Fujimoto, M., Maezawa, K., Saito, Y., Yokota, S., Asamura, K., Tanaka, T., Tsunakawa, H., Matsushima, M., Takahashi, F., Terasawa, T., Shibuya, H., Shimizu, H.

(2009) Solar-wind proton access deep into the near-Moon wake, Geophys. Res. Lett., 36, L16103, doi:10.1029/2009GL039444.

Nishino, M. N., Fujimoto, M., Saito, Y., Tsunakawa, H., Kasahara, Y., Kawamura, M., Matsushima, M., Takahashi, F., Shibuya, H., Shimizu, H., Goto, Y., Hashimoto, K., Omura, Y., Kumamoto, A., Ono, T., Yokota, S. (2013) Type-II entry of solar wind protons into the lunar wake: Effects of magnetic connection to the night-side surface, Planetary and Space Science, 87, 106-114, doi:10.1016/j.pss.2013.08.017.

Ogilvie, K. W., Steinberg, J. T., Fitzenreiter, R. J., Owen, C. J., Lazarus, A. J., Farrell, W. M., Torbert, R. B. (1996), Observation of the lunar plasma wake from the WIND spacecraft on December 27, 1994, Geophys. Res. Lett., 23, 1255-1258, doi:10.1029/96GL01069.

Poppe, A. R., Sarantos, M. Halekas, J. S., Delory, G. T., Saito, Y. Nishino, M. (2014), Anisotropic solar wind sputtering of the lunar surface induced by crustal magnetic anomalies, Geophys. Res. Lett., 41, 4865–4872, doi:10.1002/2014GL060523.

Saito, Y., S. Yokota T. Tanaka K. Asamura M. N. Nishino M. Fujimoto H. Tsunakawa H. Shibuya M. Matsushima H. Shimizu F. Takahashi T. Mukai T. Terasawa, (2008), Solar wind proton reflection at the lunar surface: Low energy ion measurement by MAP-PACE onboard SELENE (Kaguya), Geophys. Res. Lett., 35, L24205, doi:10.1029/2008GL036077.

Saito, Y., Yoshifumi Saito, Yokota, S., Asamura, K., Tanaka,T., Nishino, M. N., Yamamoto, T., Terakawa, Y., Fujimoto, M., Hasegawa, H., Hayakawa, H., Hirahara, M., Hoshino, M., Machida, S., Mukai, T., Nagai, T., Nagatsuma, T., Nakagawa, T., Nakamura, M., Oyama, K.-I., Sagawa, E., Sasaki, S., Seki, K., Shinohara, I., Terasawa, T., Tsunakawa, H., Shibuya, H., Matsushima, M., Shimizu, H., & Takahashi, F. (2010), In-flight performance and initial results of Plasma energy Angle and Composition Experiment (PACE) on SELENE (Kaguya), Space Sci. Rev., 154, 265-303, doi:10.1007/s11214-010-9647-x.

Saito, Y., Nishino, M. N., Fujimoto, M., Yamamoto, T., Yokota, S., Tsunakawa, H., Shibuya, H., Matsushima, M., Shimizu, H. & Takahashi, F. (2012), Simultaneous observation of the electron acceleration and ion deceleration over lunar magnetic anomalies, Earth Planet. Space, 64(2), 83-92, doi:10.5047/eps.2011.07.011.

Schubert, G. & Lichtenstein, B. R. (1974), Observations of moon-plasma interactions by orbital and surface experiments, Rev. Geophys. Space Phys., 12, 592-626.

Shimizu, H., Takahashi, F., Horii, N., Matsuoka, A., Matsushima, M., Shibuya, H., & Tsunakawa, H. (2008), Ground calibration of the high-sensitivity SELENE lunar magnetometer LMAG. Earth, Planets and Space, 60, 353–363, doi:10.1186/BF03352800.

Sonnerup, B. U. Ö. & Cahill, L. J. (1967), Magnetopause structure and attitude from Explorer 12 observations, J. Geophys. Res., 72(1), 171– 183, doi:10.1029/JZ072i001p00171.

Takahashi, F., Shimizu, H., Matsushima, M., Shibuya, H., Matsuoka, A., Nakazawa, S., Iijima, Y., Otake, H., & Tsunakawa, H. (2009). In-orbit calibration of the lunar magnetometer onboard SELENE (KAGUYA). Earth, Planets and Space, 61, 1269–1274.

Tsugawa, Y., Terada, N., Katoh, Ono, T., Tsunakawa, H., Takahashi, F., Shibuya, H., Shimizu, H., & Matsushima, M. (2011), Statistical analysis of monochromatic whistler waves near

the Moon detected by Kaguya, Ann. Geophys., 29, 889–893, doi:10.5194/angeo-29-889-2011.

Tsugawa, Y., Katoh, Y., Terada, N., Y., Ono, T., Tsunakawa, H., Takahashi, F., Shibuya, H., Shimizu, H., Matsushima, M., Saito, Y., Yokota, S., & Nishino, M. N. (2012), Statistical study of broadband whistler-mode waves detected by Kaguya near the Moon, Geophys. Res. Lett., 39, L16101, doi:10.1029/2012GL052818.

Tsunakawa, H., Shibuya, H., Takahashi, F., Shimizu, H., Matsushima, M., Matsuoka, A., Nakazawa, S., Otake H., & Iijima Y. (2010), Lunar magnetic field observation and initial global mapping of lunar magnetic anomalies by MAP-LMAG onboard SELENE (Kaguya), Space Sci. Rev., 154, 219-251, doi:10.1007/s11214-010-9652-0.

Tsunakawa, H., F. Takahashi, H. Shimizu, H. Shibuya, and M. Matsushima (2015), Surface vector mapping of magnetic anomalies over the Moon using Kaguya and Lunar Prospector observations, J. Geophys. Res. Planets, 120, 1160–1185, doi:10.1002/2014JE004785.

Wieser, M., Barabash, S., Futaana, Y., Holmström, M., Bhardwaj, A., Sridharan, R., Dhanya, M.B., Wurz, P., Schaufelberger, A., Asamura, K. (2009), Extremely high reflection of solar wind protons as neutral hydrogen atoms from regolith in space, Planet. Space Sci., 57, 2132-2134, doi:10.1016/j.pss.2009.09.012.

Wieser, M., Barabash, S., Futaana, Y., Holmström, M., Bhardwaj, A., Sridharan, R., Dhanya, M.B., Wurz, P., Schaufelberger, A., Asamura, K. (2011), Erratum to “Extremely high reflection of solar wind protons as neutral hydrogen atoms from regolith in space”, Planet. Space Sci., 57, 798-799, doi:10.1016/j.pss.2011.01.016.

Figure Captions

Figure 1. Examples of the low-frequency waves detected by Kaguya at 100 km altitude above the lunar surface. (a) Ultra-low-frequency waves at 0.010–0.012 Hz and (b) whistler-mode waves at 1.1–1.4 Hz generated by the reflected ions. (c) Non-monochromatic extremely low-frequency waves generated by the reflected electrons. The red (blue) bars at the bottom of each spectrum indicate that the linearly extrapolated line of force of the magnetic field at the spacecraft intersects the dayside (nightside) surface of the moon.

Figure 2. Diffuse ELF waves observed by Kaguya at 100 km altitude above the moon on March 8, 2008. (a) Power density of the magnetic fluctuation. (b) Magnetic connection of Kaguya to the nightside (blue) or dayside (red) surface of the moon estimated by the linear extrapolation of the line of force of the magnetic field at Kaguya. (c) Sense of rotation of the magnetic field variation with respect to the background magnetic field (red for right-hand and blue for left-hand), (d) the angle between the **k** vector and the background magnetic field $\mathbf{B}_0$ for the Fourier components with a power density larger than 5×10^{-3} $\mathrm{nT}^2/\mathrm{Hz}$. (e) Angle between the **k** vector and the x_{sse} axis of the selenocentric solar ecliptic (sse) coordinate system. (f) Position of Kaguya ($x_{sse}, y_{sse}, z_{sse}$) together with the distance $\sqrt{y_{sse}^2 + z_{sse}^2}$ from the x_{sse} axis. (g) 32 s-averaged background magnetic field. (h) Omni-directional energy–time spectrogram of the ions from the IEA sensor of the PACE looking at the zenith direction and (i) from the IMA sensor facing the lunar surface.

Figure 3. Kaguya's position at the diffuse ELF wave detection on March 8, 2008. (a) Position of the moon in geocentric solar ecliptic (gse) coordinates. (b–d) Kaguya's position projected on the (b) x–y, (c) x–z, and (d) y-z planes of the selenocentric solar ecliptic (sse) coordinate system.

Figure 4. Spectra of the magnetic field variation observed by Kaguya around the moon on March 8, 2008. (a) Quiet period from 6:30:22 to 6:30:54. (b) Diffuse ELF wave period from 7:08:12 to 7:08:44. The black curves are the power density resulting from the Fourier transform applied for every 32 s of 32 Hz magnetic field data. The red lines depict the linear fit to the observed spectra in the low-frequency range from 0.031 Hz to 1 Hz. The power density of the higher-frequency range in panel (a) gives the noise level measurement. The enhancements in panel (b) over the frequency range from 4 Hz to 16 Hz are significantly higher than the noise level.

Figure 5. Kaguya's position during the diffuse ELF wave event on March 8, 2008 projected onto the map of the lunar crustal magnetic field. The colors indicate the magnetic field magnitude at 0 km altitude (Tsunakawa et al., 2015) on the Lambert azimuthal equal area projection. Kaguya's position (red crosses) is plotted every 1 min from 5:11 to 5:17 and 7:03 to 7:13.

Figure 6. A diffuse ELF event observed by Kaguya on June 14, 2008. See the legend of Figure 2.

Figure 7. Kaguya's position at the diffuse ELF wave detection on June 14, 2008. (a) Position of the moon in geocentric solar ecliptic (gse) coordinates. (b–d) Kaguya's position projected on the (b) x–y, (c) x–z, and (d) y–z planes of the sse coordinate system.

Figure 8. Magnetic connection between Kaguya and the lunar surface at 20:50 on June 14, 2008. Kaguya is represented by a cube (not in scale). The line of force of the magnetic field observed at Kaguya is represented by a purple bar extending from Kaguya. The magnetic connection to the lunar surface is examined. The red, green, and blue lines indicate the x_{ME}, y_{ME}, and z_{ME} axes, respectively, of the mean Earth/Polar Axis (ME) reference system, in which the x_{ME} axis is defined by the mean Earth direction, and the z_{ME} axis is defined by the mean rotational pole (LRO Project and LGCWG, 2008). The orange line extending from the equator to the lower left direction indicates the Sun's direction. The lunar surface is color-coded with the magnitude of the lunar crustal field at 0 km altitude (Tsunakawa et al., 2015).

Figure 9. Kaguya's position and the lunar crustal magnetic field on the northern hemisphere at 0 km altitude (Tsunakawa et al., 2015). Kaguya's position from 20:40 to 20:59 is plotted every 1 min on the Lambert azimuthal equal area projection.

Figure 10. Schematic of the observed bandwidth of the Doppler-shifted waves. The curves represent the dispersion diagrams for the plasma waves in the extremely low-frequency range with a positive ω for the right-hand polarized waves and a negative ω for the left-hand polarized waves propagating parallel to the background magnetic field. The solid lines depict the cyclotron resonance conditions. The dashed lines represent the Doppler shifts. In (a) the heavily Doppler-shifted case, the bandwidth is narrowed, and the polarization is reversed. In (b) the slightly Doppler-shifted case, the bandwidth remains broad, and the polarization remains right-handed.

Figure 11. Dispersion relation of the whistler-mode wave, cyclotron resonance condition, and Doppler shift relation for the diffuse ELF waves on 20:58 of June 14, 2008. The angular frequency is normalized by the magnitude of the ion cyclotron frequency $|\Omega_i|$. The wave number is normalized by $|\Omega_i|/c$, where c is the speed of light.

Figure 12. Dispersion diagram, cyclotron resonance condition, and Doppler shift for the diffuse ELF waves on 7:05 of March 8, 2008. See the legend of Figure 11.

Figure 13. Schematic of the whistler-mode wave propagating parallel to the magnetic field convected by the solar wind. The reflected ion trajectory is not in the exact direction. The position and size of Kaguya are not in scale.

Figure 1.

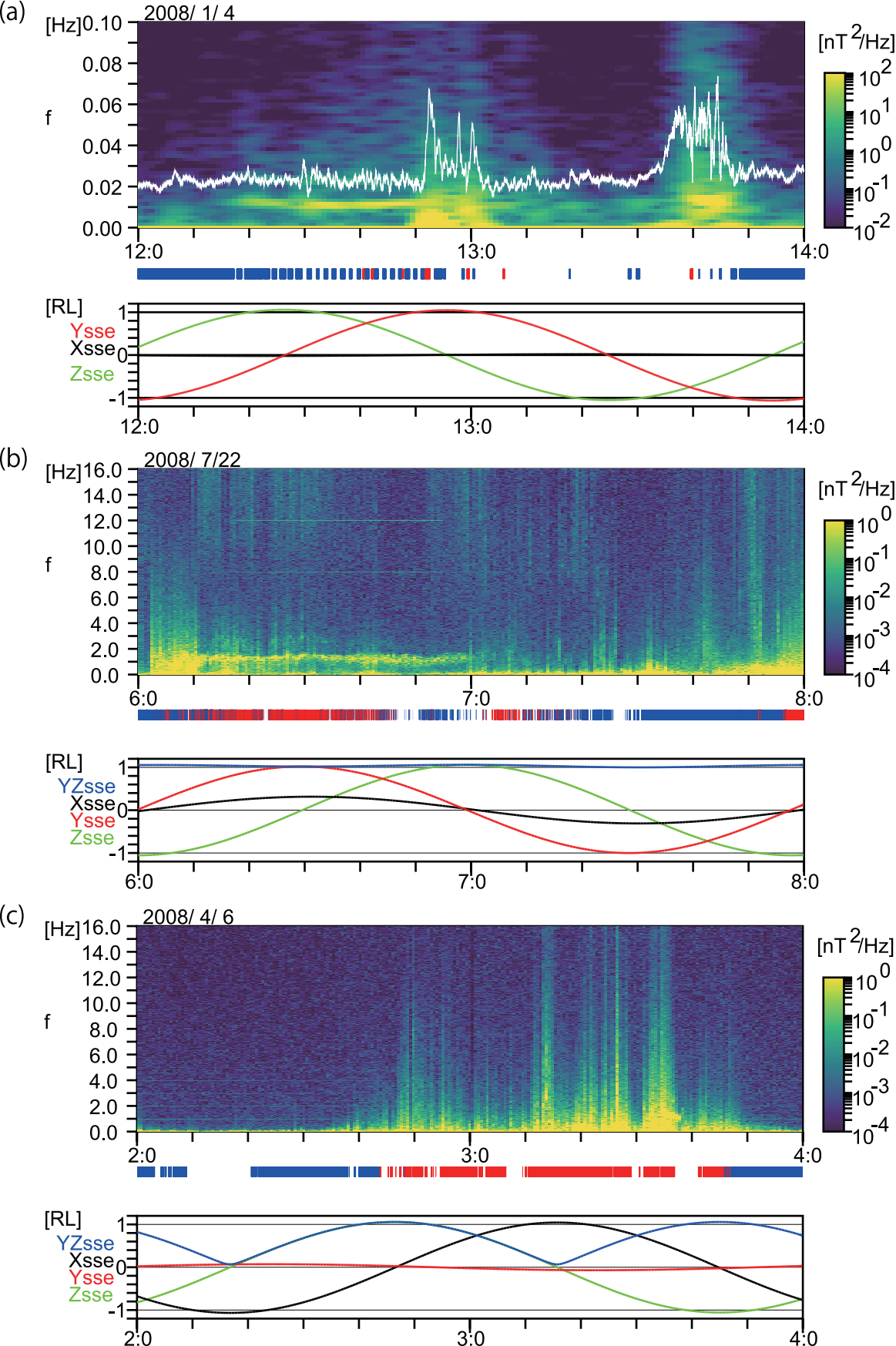
(a)
2008/ 1/ 4
[Hz]
f
0.10
0.08
0.06
0.04
0.02
0.00
12:0
13:0
14:0
[nT 2/Hz]
10 2
10 1
10 0
10 -1
10 -2
[RL]
Ysse
Xsse
Zsse
1
0
-1
12:0
13:0
14:0
(b)
2008/ 7/22
[Hz]
f
16.0
14.0
12.0
10.0
8.0
6.0
4.0
2.0
0.0
6:0
7:0
8:0
[nT 2/Hz]
10 0
10 -1
10 -2
10 -3
10 -4
[RL]
YZsse
Xsse
Ysse
Zsse
1
0
-1
6:0
7:0
8:0
(c)
2008/ 4/ 6
[Hz]
f
16.0
14.0
12.0
10.0
8.0
6.0
4.0
2.0
0.0
2:0
3:0
4:0
[nT 2/Hz]
10 0
10 -1
10 -2
10 -3
10 -4
[RL]
YZsse
Xsse
Ysse
Zsse
1
0
-1
2:0
3:0
4:0

Figure 2.

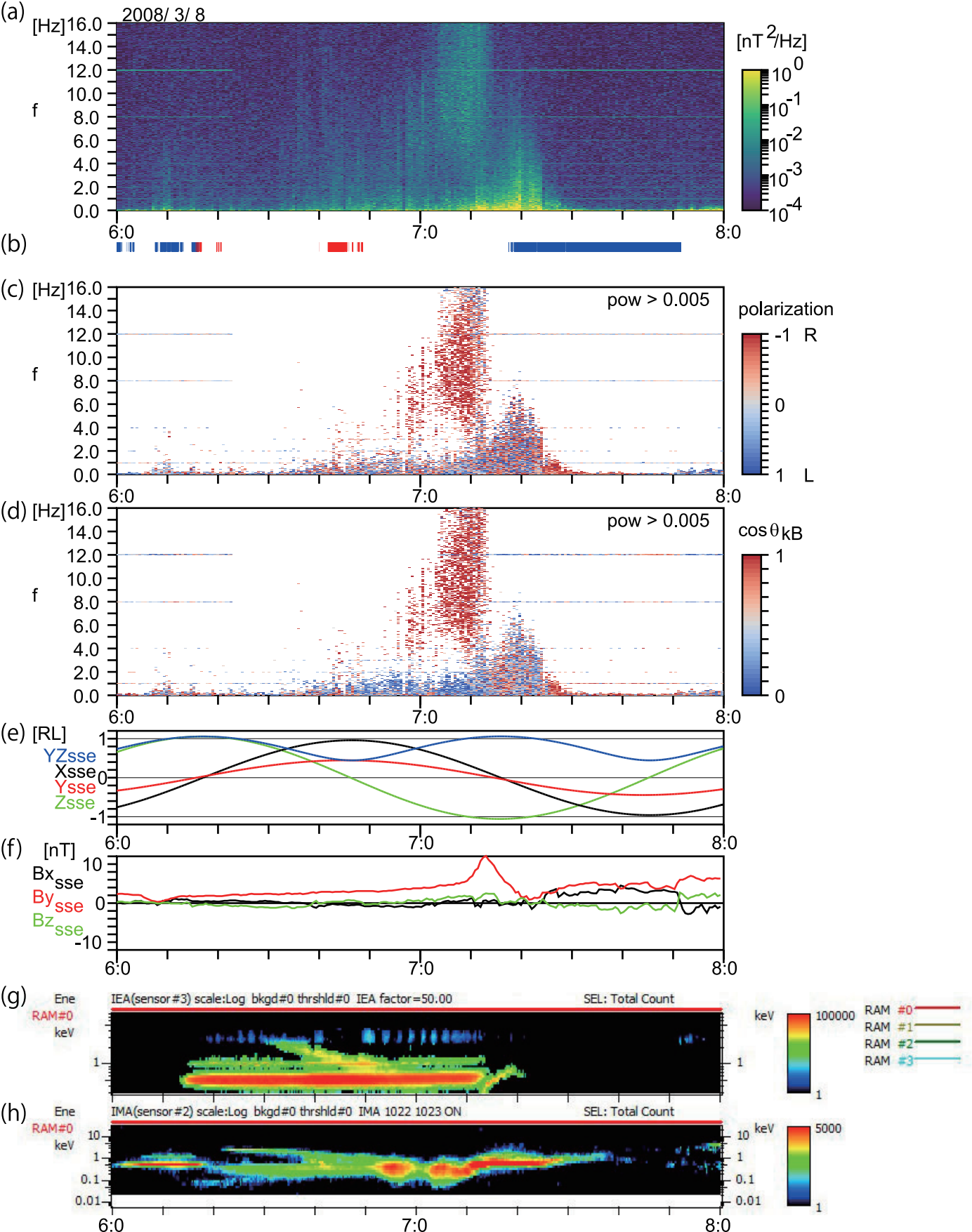
(a)
2008/ 3/ 8
[Hz]
f
[nT 2/Hz]
(b)
(c)
pow > 0.005
polarization
-1 R
0
1 L
(d)
pow > 0.005
cos θ kB
(e) [RL]
YZsse
Xsse
Ysse
Zsse
(f) [nT]
Bx sse
By sse
Bz sse
(g)
Ene
RAM#0
keV
IEA(sensor#3) scale:Log bkgd#0 thrshld#0 IEA factor=50.00
SEL: Total Count
RAM #0
RAM #1
RAM #2
RAM #3
(h)
IMA(sensor#2) scale:Log bkgd#0 thrshld#0 IMA 1022 1023 ON
6:0
7:0
8:0

Figure 3.

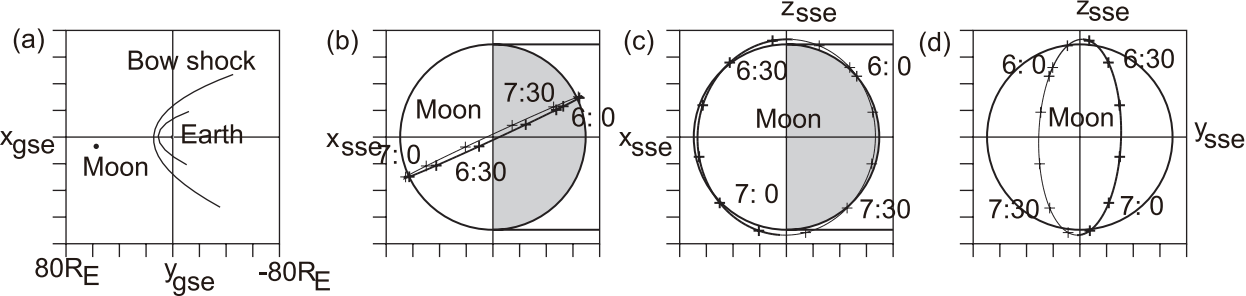
(a)
Bow shock
Earth
Moon
x_{gse}
80R_E
y_{gse}
-80R_E
(b)
Moon
7:30
6: 0
7: 0
6:30
x_{sse}
(c)
z_{sse}
6:30
6: 0
Moon
7: 0
7:30
x_{sse}
(d)
z_{sse}
6: 0
6:30
Moon
7:30
7: 0
y_{sse}

Figure 4.

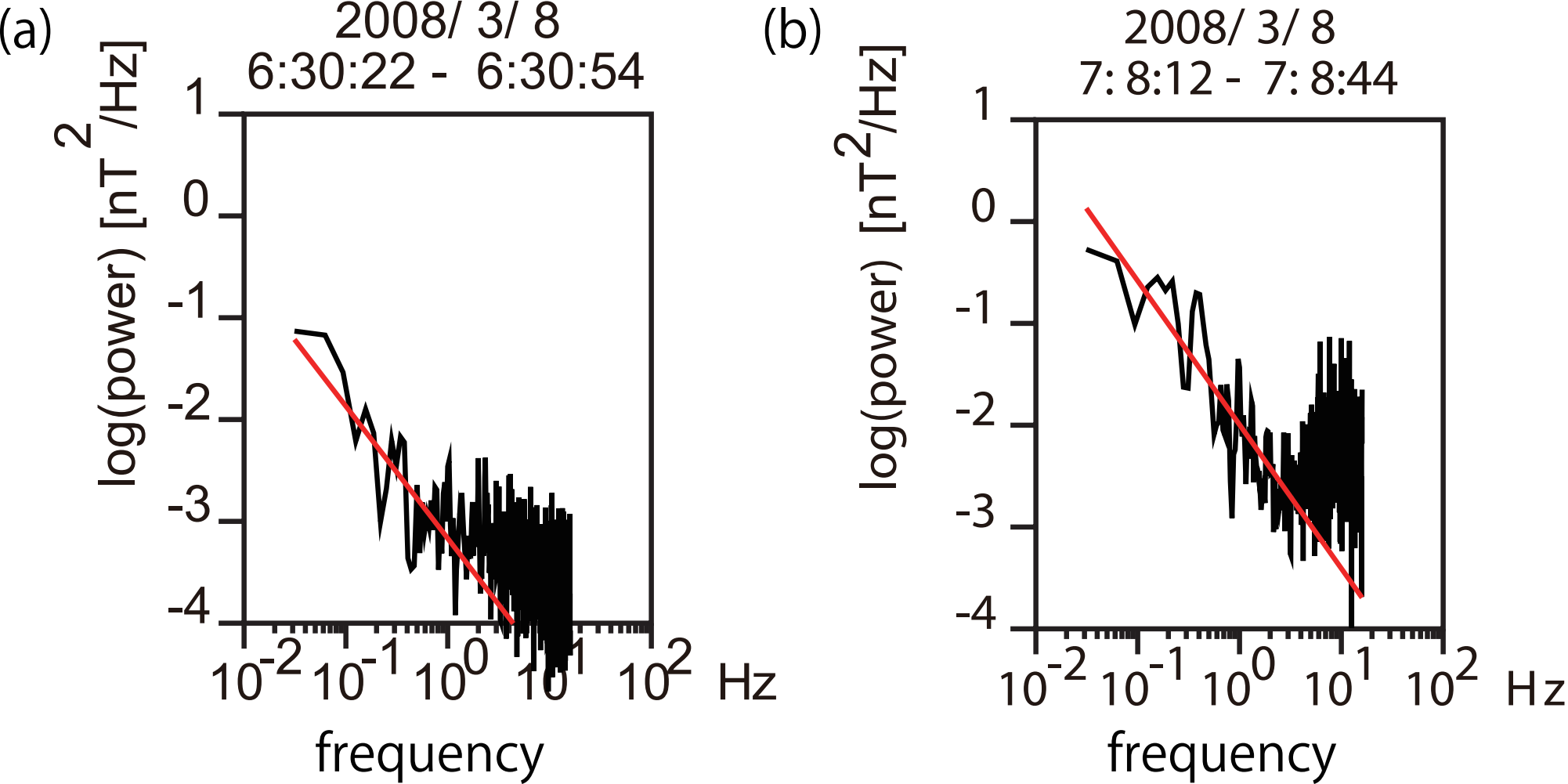
(a)
2008/ 3/ 8
6:30:22 - 6:30:54
log(power) [nT2/Hz]
1
0
-1
-2
-3
-4
10-2 10-1 100 101 102 Hz
frequency
(b)
2008/ 3/ 8
7: 8:12 - 7: 8:44
log(power) [nT2/Hz]
1
0
-1
-2
-3
-4
10-2 10-1 100 101 102 Hz
frequency

Figure 5.

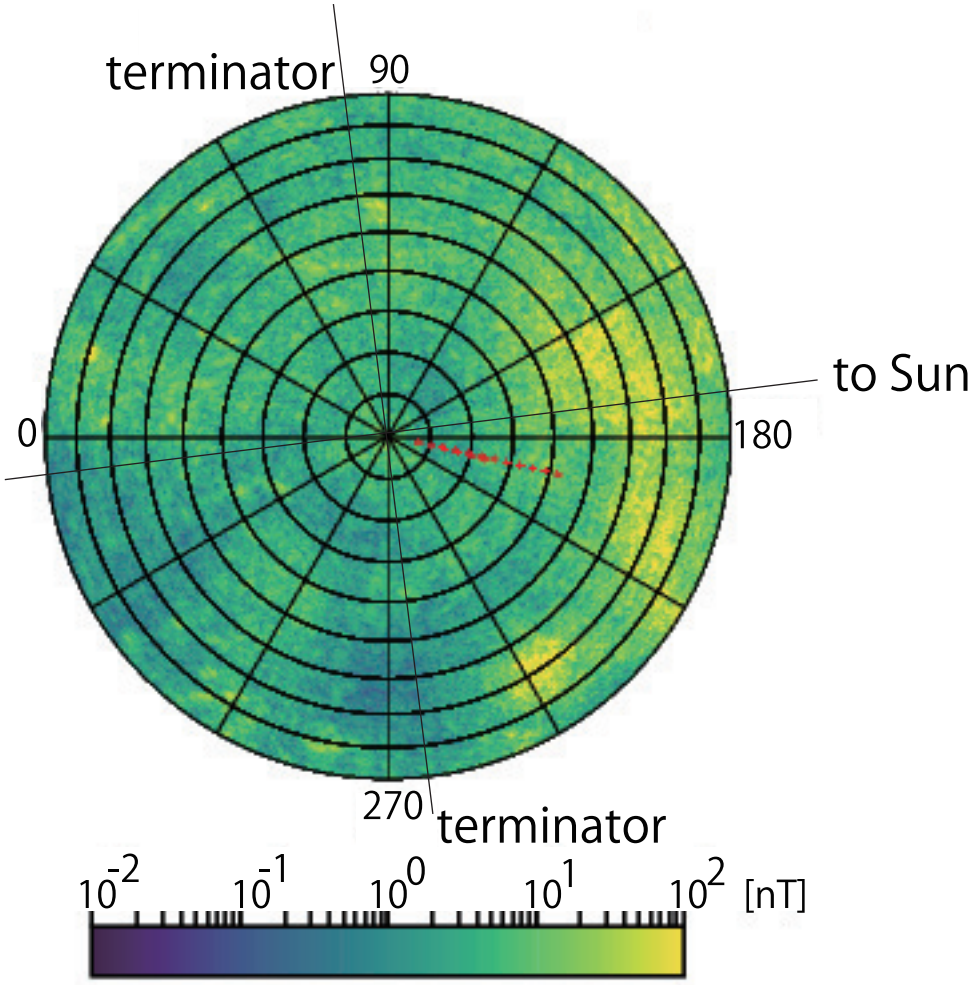
terminator
90
to Sun
0
180
270
terminator
10^{-2}
10^{-1}
10^{0}
10^{1}
10^{2}
[nT]

Figure 6.

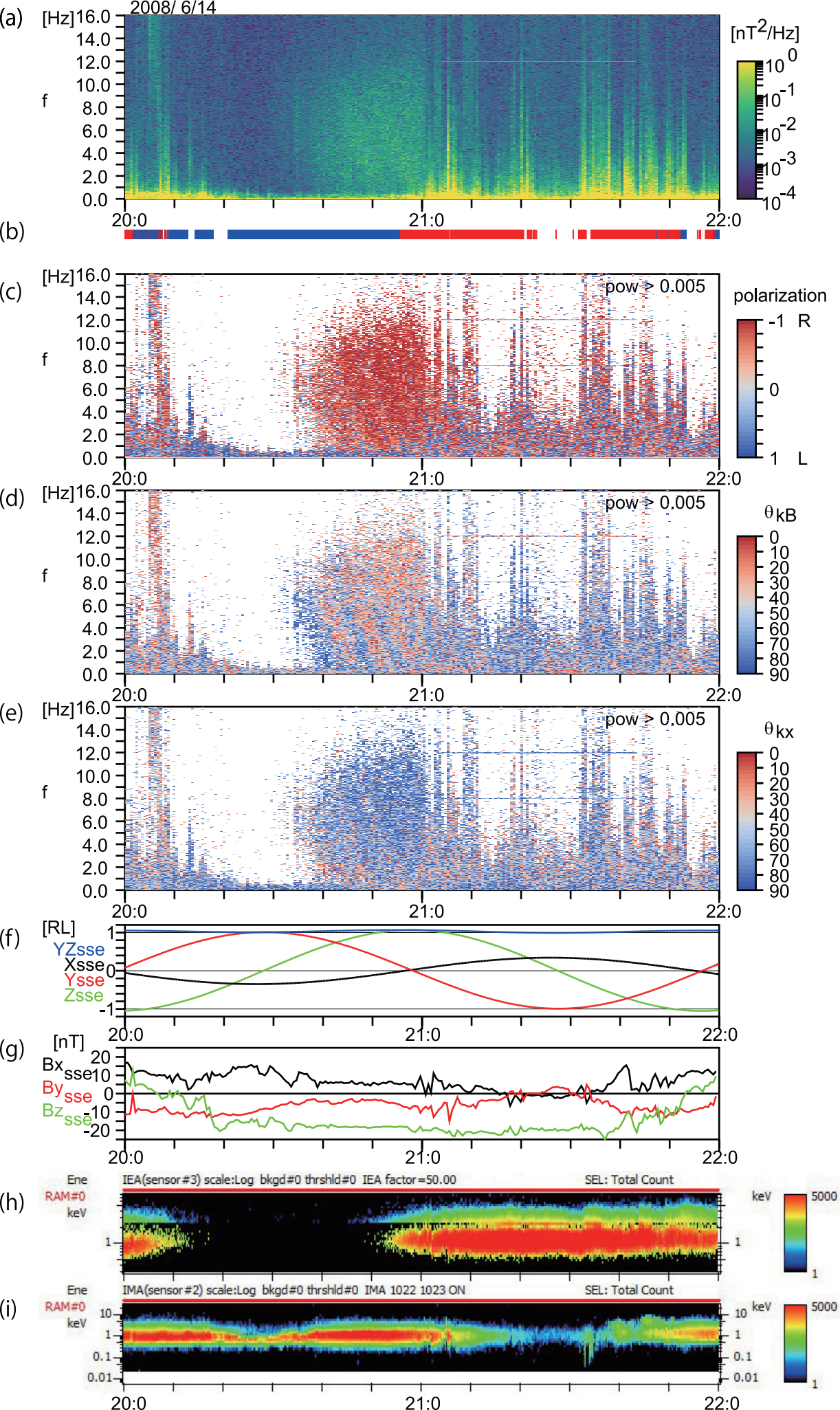
(a)
2008/ 6/14
[Hz]
f
[nT2/Hz]
(b)
(c)
pow > 0.005
polarization
R
L
(d)
θkB
(e)
θkx
(f)
[RL]
YZsse
Xsse
Ysse
Zsse
(g)
[nT]
Bxsse
Bysse
Bzsse
(h)
Ene
RAM#0
keV
IEA(sensor#3) scale:Log bkgd#0 thrshld#0 IEA factor=50.00
SEL: Total Count
(i)
IMA(sensor#2) scale:Log bkgd#0 thrshld#0 IMA 1022 1023 ON
20:0
21:0
22:0

Figure 7.

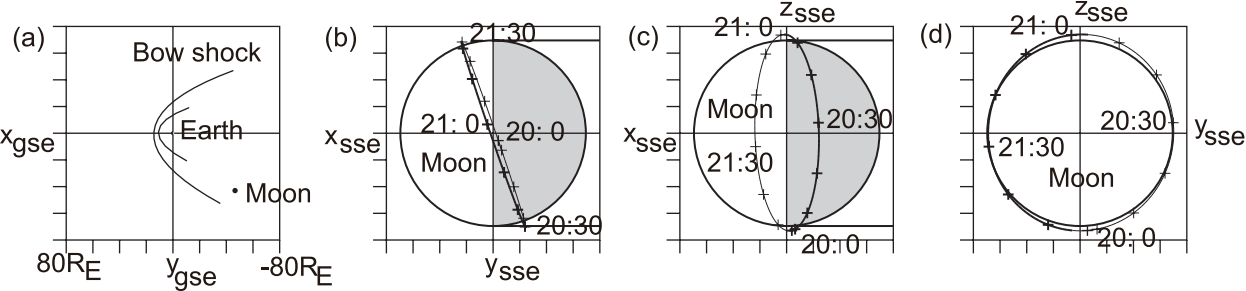
(a)
Bow shock
Earth
Moon
x_{gse}
80R_E
y_{gse}
-80R_E
(b)
21:30
21: 0
20: 0
Moon
20:30
x_{sse}
y_{sse}
(c)
21: 0
z_{sse}
Moon
20:30
21:30
x_{sse}
20:0
(d)
21: 0
z_{sse}
20:30
21:30
Moon
y_{sse}
20: 0

Figure 8.

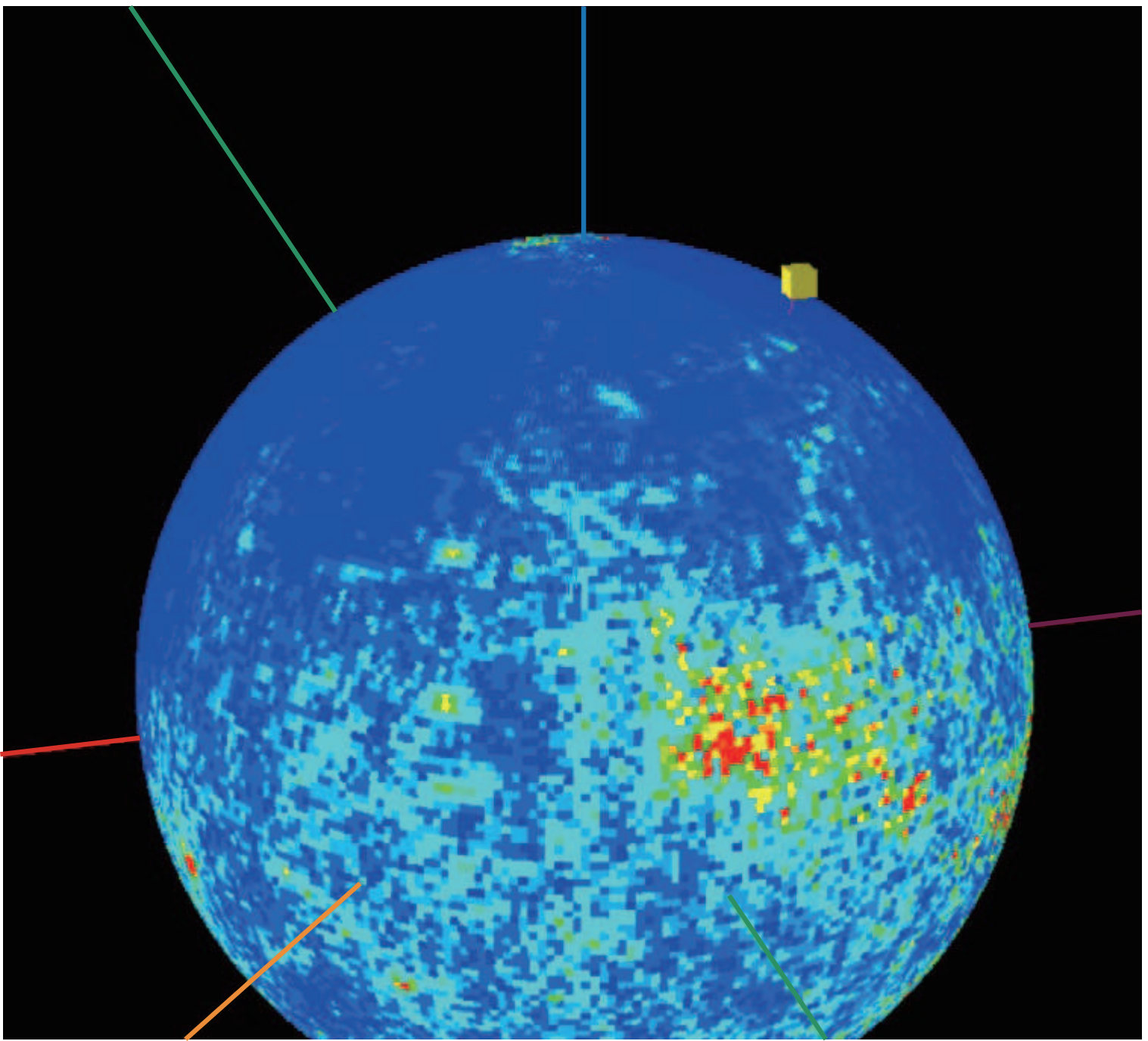

Figure 9.

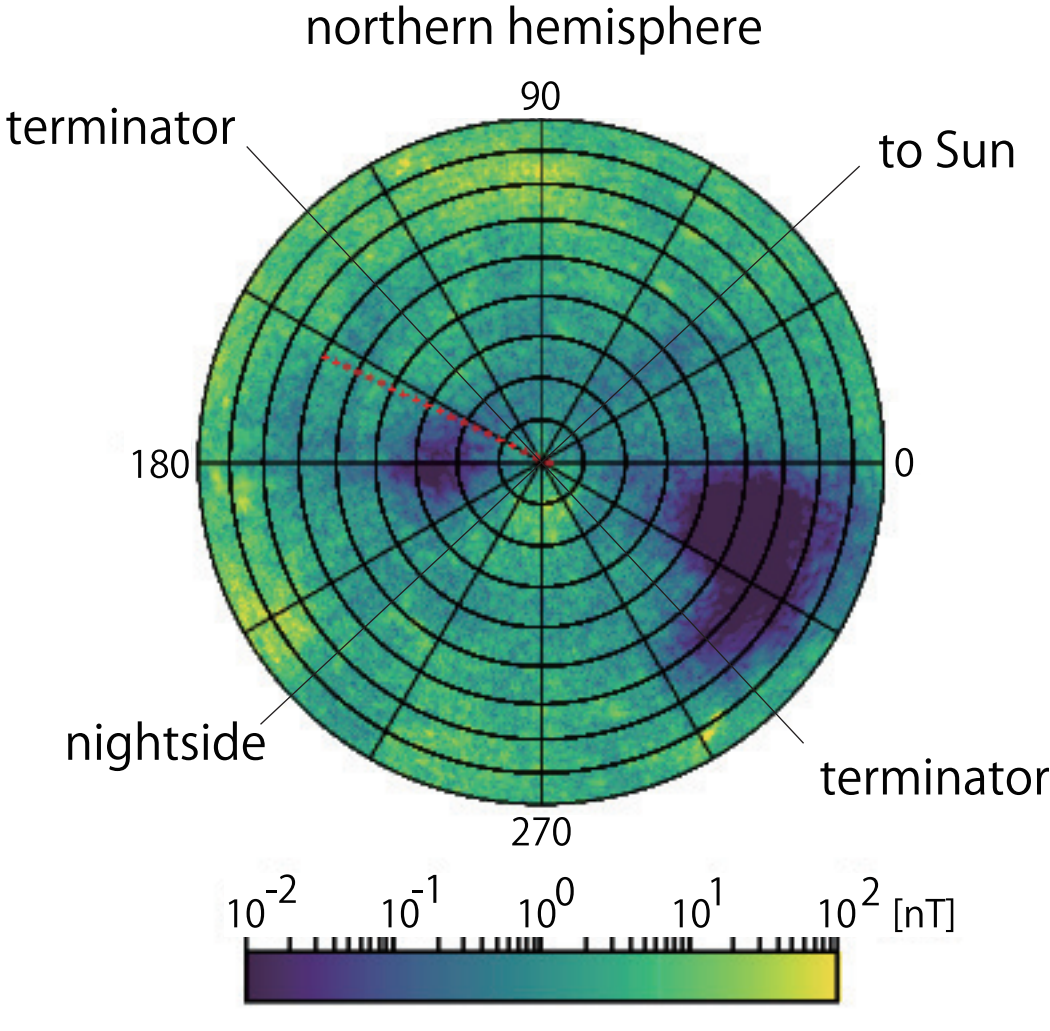
northern hemisphere
90
terminator
to Sun
180
0
nightside
terminator
270
10^-2
10^-1
10^0
10^1
10^2 [nT]

Figure 10.

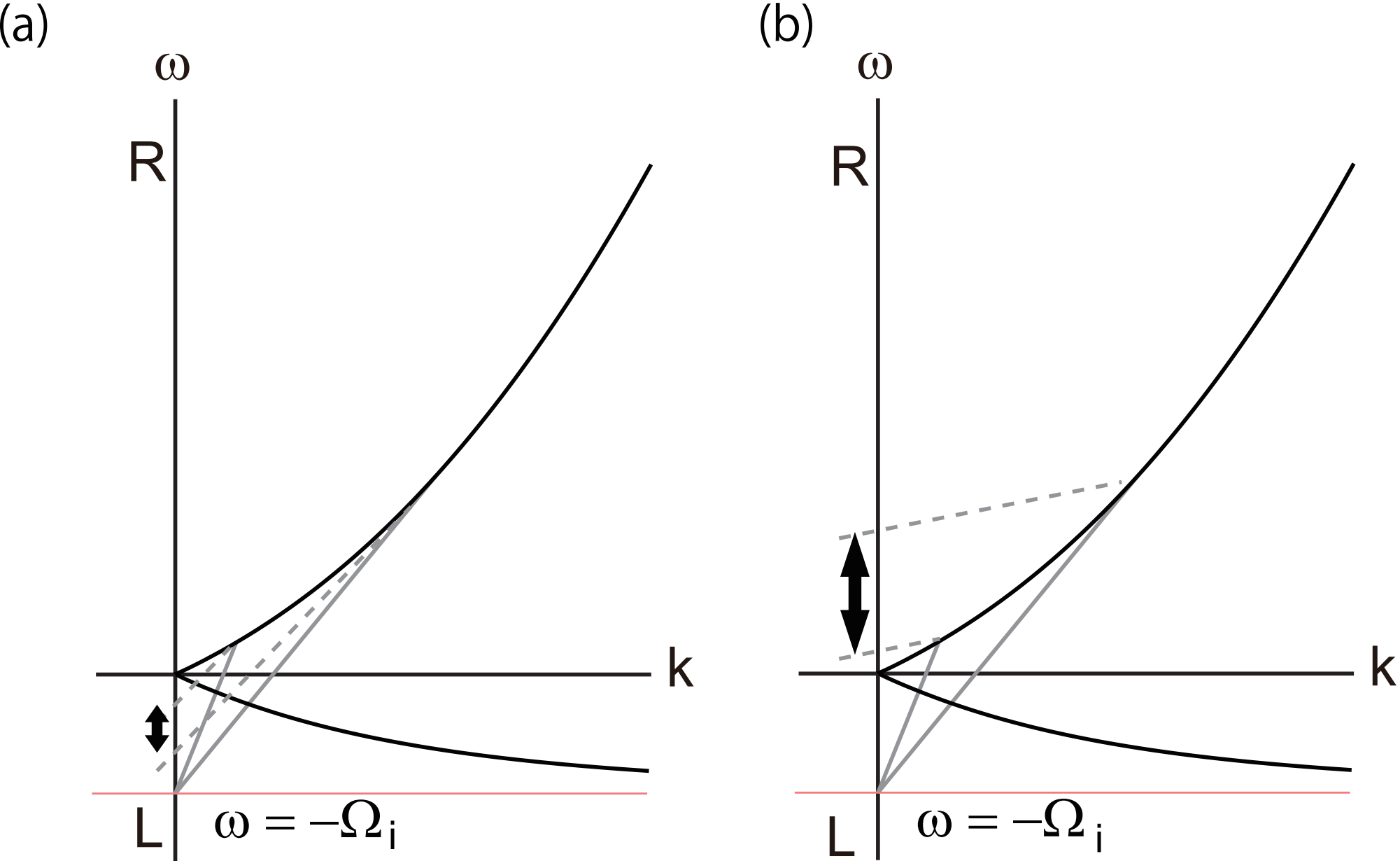
(a)
ω
R
k
L
ω = −Ω_i
(b)
ω
R
k
L
ω = −Ω_i

Figure 11.

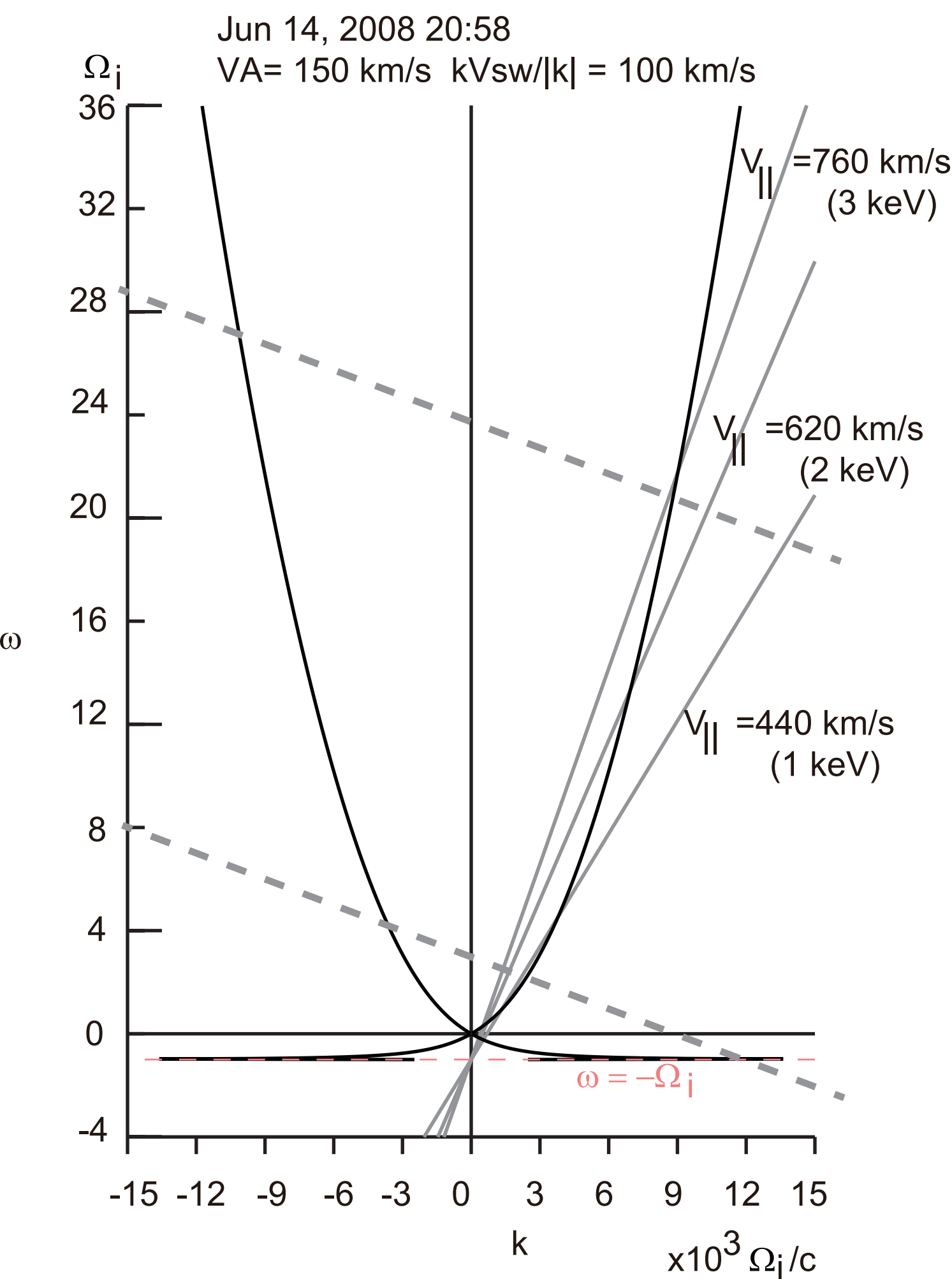
Jun 14, 2008 20:58
VA= 150 km/s kVsw/|k| = 100 km/s
Ωi
36
32
28
24
20
16
12
8
4
0
-4
ω
V|| =760 km/s
(3 keV)
V|| =620 km/s
(2 keV)
V|| =440 km/s
(1 keV)
ω = −Ωi
-15 -12 -9 -6 -3 0 3 6 9 12 15
k
x10^3 Ωi/c

Figure 12.

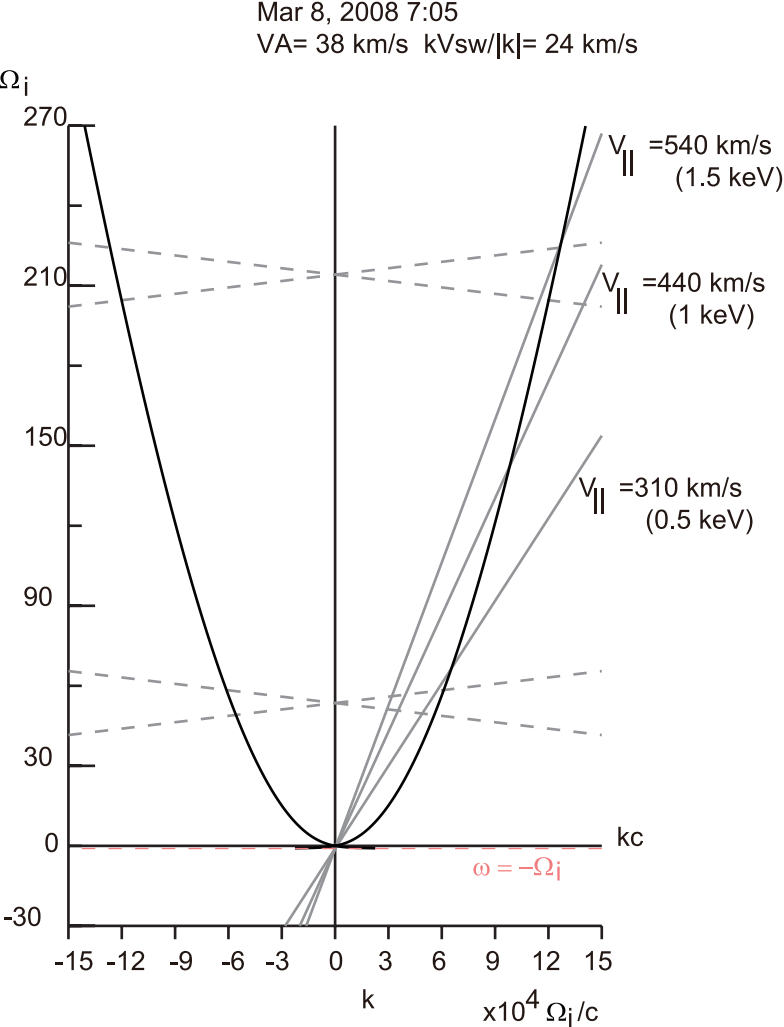
Mar 8, 2008 7:05
VA= 38 km/s kVsw/|k|= 24 km/s
Ωi
270
210
150
90
30
0
-30
-15 -12 -9 -6 -3 0 3 6 9 12 15
k
x10^4 Ωi/c
V|| =540 km/s
(1.5 keV)
V|| =440 km/s
(1 keV)
V|| =310 km/s
(0.5 keV)
kc
ω = −Ωi

Figure 13.

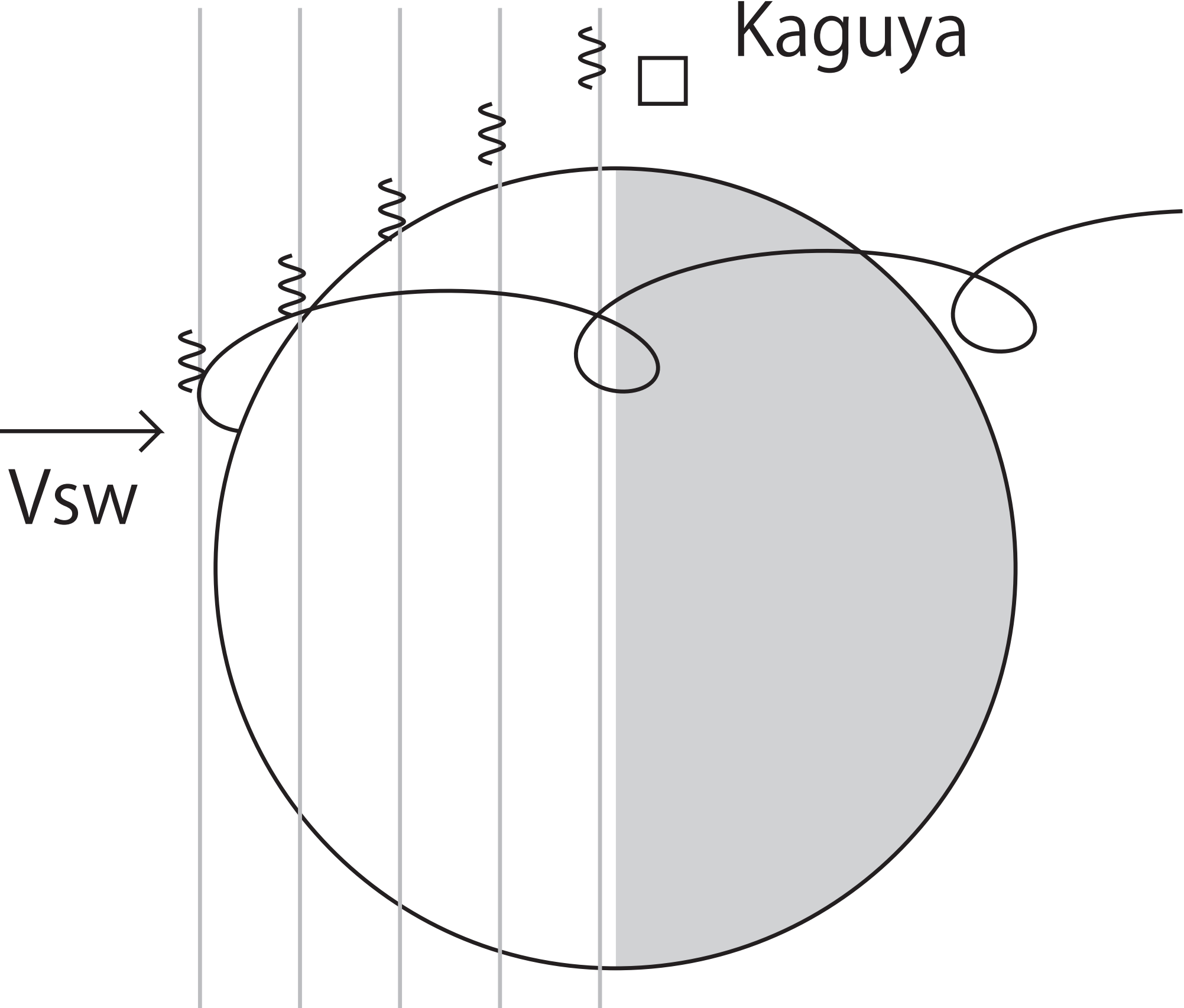
Kaguya
Vsw